Taylor instability of finite surface waves

By H. W. EMMONS, C. T. CHANG and B. C. WATSON
Harvard University, Cambridge, Mass.

(Received 20 May 1959)

The instability of the accelerated interface between a liquid (methanol or carbon tetrachloride) and air has been investigated experimentally for approximate sinusoidal disturbances of wave-number range from well below to well above the cut-off. The growth rates are measured and compared with theoretical results. A third-order theory shows the phenomena of overstability which is found in the experimental results. Some measurements of later stages of growth agree moderately well with the available theory and disclose some additional phenomena of bubble competition, Helmholtz instability with transition to turbulence, and jet instability with production of drops.

1. Introduction

If a glass were held upside down with water held magically, in its usual position, and then released, the water would fall out. This process occurs in underwater explosions, in the acceleration by combustion of liquid fuels, in the acceleration of stellar material, and, perhaps, in the molten layer, if any, on the leading edge of a blunt re-entry body. These acceleration-unstable liquid surface phenomena were studied by G. I. Taylor in the early 1940's with the first publication in 1950. He showed that in the absence of viscosity and surface tension all small surface irregularities are unstable and grow in time.

An initial test of the correctness of Taylor's ideas, apart from comparison with explosion photographs where the accelerations were uncertain, was made by Lewis (1950). As discussed later, the agreement was well within experimental scatter, but the investigation was limited to a wavelength (or acceleration) range in which the effect of surface tension was slight.

That surface tension and viscosity have modifying effects is clear, and it was shown by Bellman & Pennington (1954) that surface tension produces a cut-off wave-number (or wavelength) above which the surface disturbance merely oscillates and below which the disturbances grow. Viscosity, on the other hand, merely decreases the rate of growth at low wave-number and causes damping of the oscillatory solutions at high wave-numbers.

Allred & Blount (1953) with apparatus similar to that used by Lewis have, by using two fluids with densities close to each other to reduce the growth rate, studied the stability in a range where surface tension would be expected to play a part. Their results indicated a growth rate appreciably lower than the rate indicated by Bellman & Pennington's theory.

Experimental results show that the linear growth discussed in the theories can

apply only for very short times. The liquid surface rapidly changes to liquid spikes falling into the gas and gas bubbles rising* through the liquid.

Attempts to analyse these later developments have been made by Ingraham (1954) analytically, and Pennington *et al.* (1953) numerically. Both analyses showed the type of distortion of sinusoidal waves as observed, but neither carried the work to very large displacements.

Certain large displacement effects have been examined. Davies & Taylor (1950) studied the constant rate of rise of bubbles through a stationary liquid, while Birkhoff (1954) and Garabedian (1957) have computed with high precision the bubble-rise velocity.

On the other hand, the spikes have been shown analytically by Carrier (1953) and numerically by Pennington *et al.* (1953) to be simply left behind. Thus relative to the acceleration field the spikes are simply in free fall.

These very approximate analyses fall far short of describing the later stages of development. The régime established after spikes and rising bubbles have appeared could remain until the spikes 'hit the bottom', while the bubbles 'rise to the top'; but in fact such a motion is found unstable. The rising bubbles compete with one another, the large ones growing at the expense of the small ones. Some indications of this type of behaviour is given in figure 1 (plate 1). The gas-liquid interface on the sides of the spikes and bubbles are in relative (tangential) motion which produces additional surface instability of the Helmholtz type. These experimentally observed phases have been recognized by Lewis (1950) and Birkhoff (1954), but no detailed attempt to obtain analytical nor experimental knowledge of the processes has been made. In particular the final stage of mixing could only be of interest in its various statistical properties (it being hopelessly complex for detailed description), yet it could be analysed only by a statistic which was strongly biased by spacial and time variations of very large magnitude.

2. Growth of surface waves

A. *Theoretical consideration—finite waves with surface tension*

For the purposes of analysis, we shall treat the medium as a non-viscous, incompressible fluid. Surface tension is included. The upper fluid is taken as air whose density we may neglect relative to that of the liquid. The flow-field is assumed to be two-dimensional, with the x'-axis taken in the unperturbed plane of the interface. For simplicity, we shall assume that the motion of the whole system is started from rest and the initial surface disturbance is a simple sinusoidal standing wave with amplitude η_0' and wave-number k'. For the proper interpretation of the results, all the physical parameters concerned will be expressed in dimensionless forms. As standards of measurement we shall take the wave-number k' and the wave velocity $\sqrt{(g'/k')}$, of the initial disturbances, as scales of length and velocity, respectively, where g' is the acceleration relative to a force-free frame of reference. $\rho g'$ is a virtual gravity force taken as positive in a direction normal to the surface

* The terms 'rising' and 'falling' refer of course to the familiar gravity effects on an upside down glass of water. For the general case, 'downwards' is the direction of the effective gravity component, directed for instability from the heavier toward the lighter medium.

from the heavier toward the lighter medium. Thus for liquids at rest on the surface of the earth, $g' = -981\ \mathrm{cm/sec^2}$.

The dimensionless independent variables of the problem will be taken as

$$x = k'x', \quad y = k'y', \quad t = \sqrt{(+g'k't')}. \tag{2.1}$$

In terms of these dimensionless variables, the governing equations and the boundary conditions for the velocity potential $\phi(x, y, t)$ (defined by $\mathbf{u} = -\operatorname{grad}\phi$) and the surface displacement $\eta(x, t)$ in the y-direction are:

Governing equations:

$$\phi_{xx} + \phi_{yy} = 0$$

for $$\infty > x > -\infty, \quad \eta > y > -\infty, \quad t \geqslant 0. \tag{2.2}$$

Boundary conditions:

The liquid surface moves with the liquid,

$$\eta_t - \eta_x\phi_x + \phi_y = 0. \tag{2.3}$$

The pressure in the liquid differs from atmospheric by the effect of surface tension and the curvature,

$$-\eta - \phi_t + \tfrac{1}{2}(\phi_x^2 + \phi_y^2) = k^2[\eta_{xx}(1+\eta_x^2)^{-\frac{3}{2}}] \tag{2.4}$$

on $y = \eta(x, t)$.

Initial conditions:
$$\eta(x, 0) = \eta_0 \cos x, \tag{2.5}$$

$$\eta_t(x, 0) = 0. \tag{2.6}$$

In equation (2.4) k is given by,

$$k = \frac{k'}{k_c'}, \tag{2.7}$$

where k_c', the cut-off wave-number, is given by

$$k_c' = \sqrt{\frac{\rho g'}{T}}, \tag{2.8}$$

where T is the surface tension. The parameter k can also be interpreted as the ratio of the surface tension forces to the gravity forces.

In order to proceed analytically, let us assume that the surface disturbance admits an expansion of the following type:

$$\eta = \sum_{r=1}^{\infty} \eta_0^r \eta_r(x, t). \tag{2.9}$$

If η_r and all its derivatives are further assumed to be of the same order of magnitude, it follows from equation (2.3) that

$$\phi = \sum_{r=1}^{\infty} \eta_0^r \phi_r. \tag{2.10}$$

Since equation (2.2) is linear, it must be satisfied by every ϕ_r. Our general scheme of solution is to introduce equations (2.9) and (2.10) into (2.3), (2.4), (2.5) and (2.6) and equate like powers of η_0 to find the corresponding boundary and initial conditions for ϕ_r and η_r. The values of ϕ_r and its derivatives required at

$y = \eta(x,t)$ are found from the values at $y = 0$ by use of Taylor expansions. We then determine each ϕ_r and η_r in succession to complete the solution. First, we have

$$\eta_r(x,0) = \begin{cases} \cos x & \text{for } r = 1, \\ 0 & \text{for } r \neq 1. \end{cases} \tag{2.11}$$

The following notation will be used throughout:

$$\eta_{r,t} \equiv \frac{\partial \eta_r}{\partial t} \quad \text{for all } r. \tag{2.12}$$

Then, the boundary conditions obtained by the above process from equations (2.3) and (2.4), wherein all quantities are evaluated at $y = 0$, are:

$$\eta_{1,t} + \phi_{1,y} = 0, \tag{2.13a}$$

$$\eta_1 + \phi_{1,t} + k^2 \eta_{1,xx} = 0, \tag{2.13b}$$

$$\eta_{2,t} + \phi_{2,y} = \phi_{1,x}\eta_{1,x} - \phi_{1,yy}\eta_1, \tag{2.13c}$$

$$\eta_2 + \phi_{2,t} + k^2\eta_{2,xx} = \tfrac{1}{2}(\phi_{1,x}^2 + \phi_{1,y}^2) - \phi_{1\ ty}\eta_1, \tag{2.13d}$$

$$\eta_{3,t} + \phi_{3,y} = \phi_{1,x}\eta_{2,x} + (\phi_{1,xy}\eta_1 + \phi_{2,x})\,\eta_{1,x} - \phi_{2,yy}\eta_1 - \tfrac{1}{2}\phi_{1,yyy}\eta_1^2 - \phi_{1,yy}\eta_2, \tag{2.13e}$$

$$\eta_3 + \phi_{3,t} + k^2\eta_{3,xx} = \phi_{1,x}\phi_{2,x} + \phi_{1,y}\phi_{2,y} + (\phi_{1,xy}\phi_{1,x} + \phi_{1,yy}\phi_{1,y})\,\eta_1 + \tfrac{3}{2}k^2\eta_{1,xx}(\eta_{1,x})^2 - \phi_{2,yt}\eta_1 - \tfrac{1}{2}\phi_{1,yyt}(\eta_1)^2 - \phi_{1,yt}\eta_2. \tag{2.13f}$$

At each step in approximation, the boundary conditions are now linear, all non-linearity involving lower-order functions which will have been determined as earlier approximations. All such terms have been placed on the right-hand side and are, at any given stage, known.

As expected, the first approximation, ϕ_1, η_1 are the solutions given earlier by Bellman & Pennington:

$$\phi_1 = -\mu_1 \sinh(\mu_1 t)\, e^y \cos x \quad (\equiv -B_{11,t} e^y \cos x), \tag{2.14a}$$

$$\eta_1 = \cosh(\mu_1 t)\cos x \qquad (\equiv B_{11}(t)\cos x), \tag{2.14b}$$

where

$$\mu_1^2 = 1 - k^2. \tag{2.14c}$$

These solutions show the phenomena of cut-off wave-number since $\mu_1 = 0$ at $k = 1$ and below this μ_1 is positive so that surface waves grow. Note that for waves shorter than the cut-off wavelength $(k > 1)\,\mu_1$ is imaginary and the waves oscillate; they are not damped.

The second approximation ϕ_2, η_2, extends the results published by Ingraham (1954) to include surface tension, although we solve only for a massless upper fluid:

$$\phi_2 = \frac{\mu_1}{4}\sinh 2\mu_1 t + \left(\frac{\mu_1}{4}\sinh 2\mu_1 t - \frac{B_{22}(t)}{2}\right) e^{2y}\cos 2x, \tag{2.14d}$$

$$\eta_2 = B_{22}(t)\cos 2x, \tag{2.14e}$$

where

$$\mu_2^2 = 2[1 - (2k)^2], \tag{2.14f}$$

$$B_{22}(t) = \frac{1}{2}\left(\frac{\mu_1}{\mu_2}\right)^2 \left\{1 + \frac{1}{4(\mu_1/\mu_2)^2 - 1}\left[\cosh 2\mu_1 t - 4\left(\frac{\mu_1}{\mu_2}\right)^2 \cosh \mu_2 t\right]\right\}. \tag{2.14g}$$

The equation of the surface shows the growth of the first harmonic while the velocity potential shows the first harmonic and a purely time-dependent term which arises because of the additional pressure in the liquid required to produce the velocity of the rising fluid. The first harmonic is seen on analysis of these expressions to grow only by energy addition from the fundamental if the first harmonic wave-number is above the cut-off (i.e. the fundamental $k > \frac{1}{2}$), while for first harmonic wave-numbers below the cut-off they grow also by direct energy addition from the acceleration field, once they are started.

The third approximation introduces some new features. When the first and second approximations are introduced into the boundary conditions, equations (2.13*e*) and (2.13*f*), they become

$$\eta_{3,t} + \phi_{3,y} = P_{31}(t)\cos x + P_{33}(t)\cos 3x, \tag{2.14h}$$

$$\eta_3 + \phi_{3,x} + k_2\eta_{3,xx} = Q_{31}(t)\cos x + Q_{33}(t)\cos 3x, \tag{2.14i}$$

where the P and Q functions of t are given in Appendix I. These equations show that as a result of the excitation of lower approximations not only a new mode appears ($\cos 3x$) but also a feedback of excitation to the fundamental ($\cos x$) occurs. The solution can be expressed as

$$\phi_3 = C_{31}(t)\cos x + C_{33}(t)\cos 3x, \tag{2.15}$$

$$\eta_3 = B_{31}(t)\cos x + B_{33}(t)\cos 3x, \tag{2.16}$$

where the B and C functions of t are given in Appendix II. The second harmonic behaves as the fundamental and first harmonic with respect to a cut-off wave-number above which it grows only at the expense of energy from the lower wave-number waves. The second harmonic is at the cut-off for the fundamental at $\frac{1}{3}$ cut-off wave-number. Thus the distortion of the fundamental changes nature at each wave-number $1/n$ $(n = 1, 2, 3, \ldots)$ as each successive harmonic changes from direct growth to becoming oscillatory.

The final solution for the growth of harmonic disturbances on the surface against air of an accelerated fluid is to the present order of approximation:

$$\eta = \sum_{r=1}^{\infty} \eta_0^r \eta_r = \eta_0 \cosh \mu_1 t \cos x + \eta_0^2 B_{22}(t)\cos 2x + \eta_0^3(B_{31}(t)\cos x + B_{33}(t)\cos 3x) + \ldots. \tag{2.17}$$

A corresponding sum holds for

$$\phi(x, y, t) = \sum_{r=1}^{\infty} \eta_0^r \phi_r = -\eta_0 \mu_1 \sinh \mu_1 t e^{y} \cos x + \eta_0^2 \left[\frac{\mu_1}{4}\sinh 2\mu_1 t + \left(\frac{\mu_1}{4}\sinh 2\mu_1 t - \frac{B_{22,t}}{2}\right) e^{2y}\cos 2x\right] + \eta_0^3(C_{31}\cos x + C_{33}\cos 3x) + \ldots. \tag{2.18}$$

These series can be expressed as Fourier series by rearrangement:

$$\eta = \sum_{m=1}^{\infty} A_m(k, t)\cos mx, \tag{2.19}$$

where $A_m(k, t) = \sum_{r=m}^{\infty} B_{rm}(k, t)\,\eta_0^r$ and the $B_{rm}(k, t)$ are given in Appendix II up to B_{33}. Thus is displayed the harmonic content of the distorted growing disturbance.

From the hyperbolic function nature of the B_{mr} functions already obtained and the manner of their formation, it appears that the entire series, if obtained, would change to a group of irrationally spaced time harmonic terms when the fundamental wave-number exceeds unity. This appears contrary to experimental results discussed in the next section. In any case, the present solution to the third approximation is still limited to small wave amplitudes; certainly not exceeding $\eta = \eta' k' = 2\pi$, i.e. the wave amplitude equal to the wavelength.

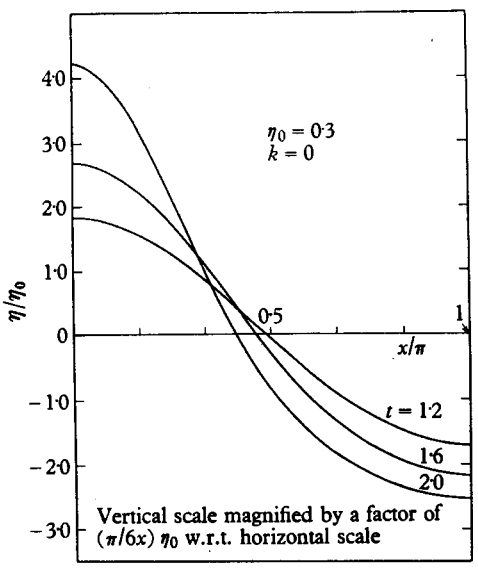

FIGURE 2. Calculated wave profiles at different times.

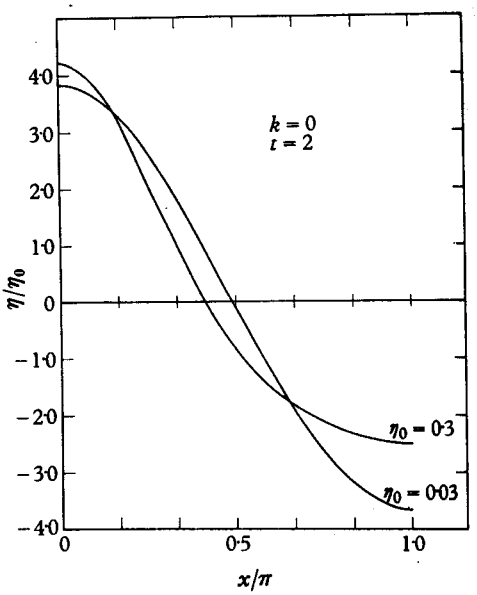

FIGURE 3. Calculated wave profiles with different initial amplitudes.

Results of the analysis indicate that in order to get a reasonable representation of the wave-form even at comparatively early stages, at least a third approximation is required. An example of the growth of a surface wave is given in figure 2 where three consecutive shapes of the surface are shown for an initial sinusoidal disturbance of amplitude $\eta_0 = 0{\cdot}3$ and wave-number $k = 0$ (i.e. the effect of surface tension has been neglected). The asymmetrical growth of the surface is clearly indicated by the narrowing of the crest and the broadening of the trough of the wave with time. The influence of the amplitude and wave-number of the initial disturbance on its subsequent growth are shown in figures 3 and 4, respectively. As is to be observed there, asymmetry of the surface occurs much earlier for initial disturbances of larger amplitudes than for those of smaller amplitudes. Disturbances having wave-numbers close to 'cut-off' values (i.e. $k = 1{\cdot}0$) are more stable than those having lower wave-numbers. Neglecting the effect of surface tension is equivalent to considering the limiting case of $k = 0$. Surface tension, therefore, has a definite stabilizing effect. Alternately, the limiting case $k = 0$ can be considered as a case of infinite acceleration for which all harmonics are below cut-off wave-number and are inherently unstable once they are started.

The present third-order theory also shows that, contrary to the prediction of a modified first-order theory (Bellman & Pennington 1954), the surface disturbance still grows at the 'cut-off' wave-number (i.e. $k = 1{\cdot}0$) in the manner given by

$$\eta = \eta_0 + \tfrac{3}{16}\eta_0^3 t^2 \cos x + \tfrac{3}{64}\eta_0^3[\cos(2\sqrt{6}t) - 1]\cos 3x. \tag{2.20}$$

The crest and trough of the wave, however, are growing at equal rates. By further increasing the wave-number of the initial disturbance, as a consequence

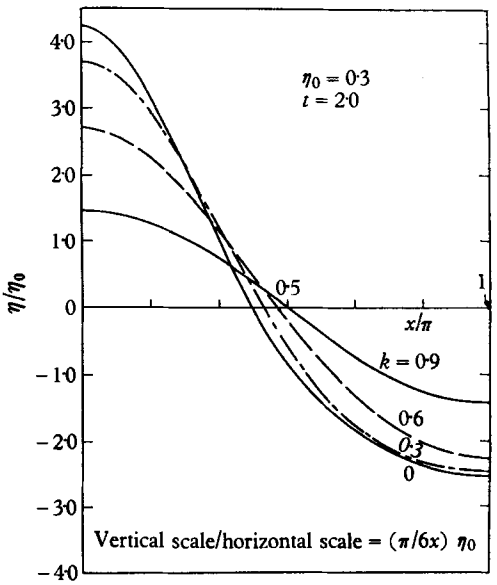

FIGURE 4. Calculated wave profiles with different wave-numbers.

	$k < 1{\cdot}0$	$k = 1{\cdot}0$	$k > 1{\cdot}0$
Taylor's original theory	$\eta_0 \exp(t)$	$\eta_0 \exp(t)$	$\eta_0 \exp(t)$
Bellman & Pennington's theory	$\eta_0 \exp\{\sqrt{(1-k^2)}\, t\}$	η_0	$\eta_0 \cos\{\sqrt{(k^2-1)}\, t\}$
Third-order theory	$\eta_0 \exp\{\sqrt{(1-k^2)}\, t\}$	$\frac{3}{16}\eta_0^3 t^2$	$e_{31}(k)\, \eta_0\{\sqrt{(k^2-1)}\, t\} \sin\{\sqrt{(k^2-1)}\, t\}$*

* Note. The term compared is the dominating one appearing in the amplitude $A_1(k, t)$ of the basic mode $A_1(k, t)\cos x$. For $e_{31}(k)$, see Appendix II.

TABLE 1. Comparison between various theories regarding the growth of the basic mode in the earlier period

of the feedback to the basic mode from the second harmonic, the surface disturbance, instead of growing exponentially in time as compared with those having wave-numbers $k < 1{\cdot}0$, tends to be 'overstabilized', i.e. it oscillates in time with an ever-increasing amplitude. As a comparison between the predictions of the various theories, we have indicated qualitatively in table 1 the behaviour of the basic mode with variation of the wave-number.

B. *Experimental apparatus*

The experimental results reported here were performed in an apparatus consisting of a glass-sided frame partially filled with liquid, a means of accelerating this frame and its contents, and various pieces of equipment for recording the behaviour of the liquid surface as the frame is accelerated. A schematic of the accelerator is given in figure 5. The frame which is accelerated is made of

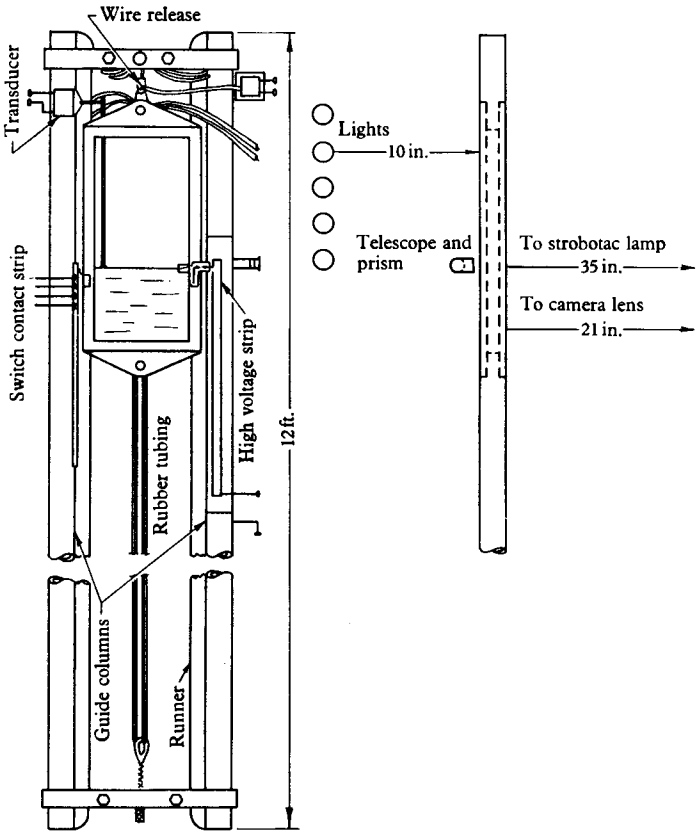

FIGURE 5. Arrangement of accelerator parts.

aluminium with a glass front and back. Its inside dimensions are 12 in. × 5 in. × 1 in. This frame is restrained to travel in a vertical direction by the two guide columns.

At the start of an experimental run the frame is held at the top of the guide columns by a steel wire while tension is applied to the rubber tubes attached to the bottom of the frame. To begin the run an electric current is passed through the steel wire, melting it and releasing the frame. After the frame has left the area of interest another set of rubber tubes attached to the upper end of the frame comes into play and arrests the moving frame.

In order to provide an initial disturbance to the surface of the liquid contained in the frame, a small paddle, its blade resting at the surface, is oscillated by a transducer driven by an audio oscillator and amplifier.

An indication of the initial amplitude of the travelling wave created by the paddle is obtained by observing the surface profile with a 30-power microscope. A stroboscope, flashing at a frequency close to the frequency at which the waves pass a fixed point, provides the illumination and creates the impression of a slowly moving wave profile which may be measured by means of a graduated reticle in the microscope.

Photography is used for recording the time and position of the surface waves and also the position of the frame at millisecond intervals. A camera is placed in

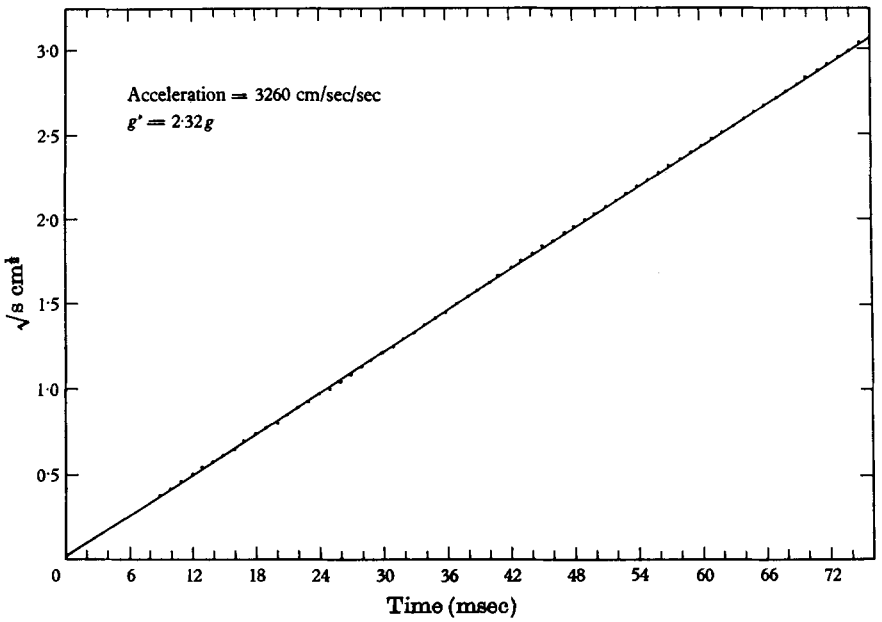

FIGURE 7. Square root of frame displacement *vs* time.

front of the frame, while behind the frame are positioned ten flash bulbs which are fired by switches tripped by the descending frame. Also located on the frame is a spark gap at which appears a spark discharge every millisecond. Because the camera shutter is open during the time that the frame is descending the film records: (*a*) the sparks giving the position of the frame every millisecond, (*b*) the ten positions of the interface at the times the flash bulbs were fired, and (*c*) the position of the spark gap at the time of the firing of the flash bulbs. The images of (*b*) and (*c*) above allow a precise determination of the relative times of the several events. A typical photograph is given in figure 6 (plate 2).

The analysis of the film by travelling microscope and photographic enlarger provides the quantitative data. The travelling microscope is used to measure the position of the spark discharges, the wavelengths, and the wave amplitudes in the earliest stage of growth. The enlarger is used in the study of the later stages of growth.

By plotting the square root of the distance from the initial position to the individual spark discharges against time (figure 7), the rate of acceleration and the relative time at which the acceleration began is obtained.

From extreme enlargements of the wave-forms of the later stages of growth an indication of the wave behaviour is obtained. A measurement of the distance from the wave spike or crest and of the bottom of the wave troughs from a mean horizontal line is made. The mean horizontal line is established by making the cross-sectional area occupied by the spikes equal to the area of the vacuated fluid in the troughs. This definition of a 'mean horizontal line' is used instead of a fixed line on the frame, because the meniscus growth changes the mean level of the waves relative to the frame. Figure 8 is an illustration of this later growth.

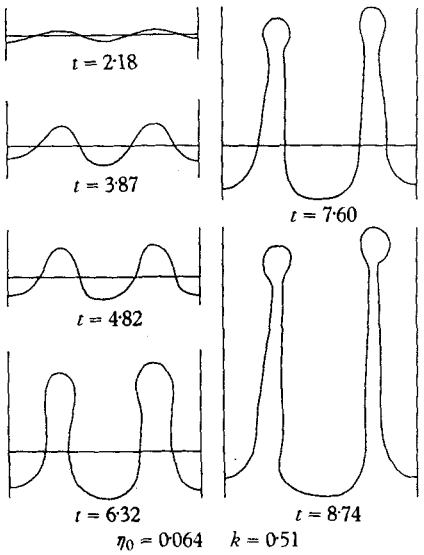

FIGURE 8. Later growth outlines.

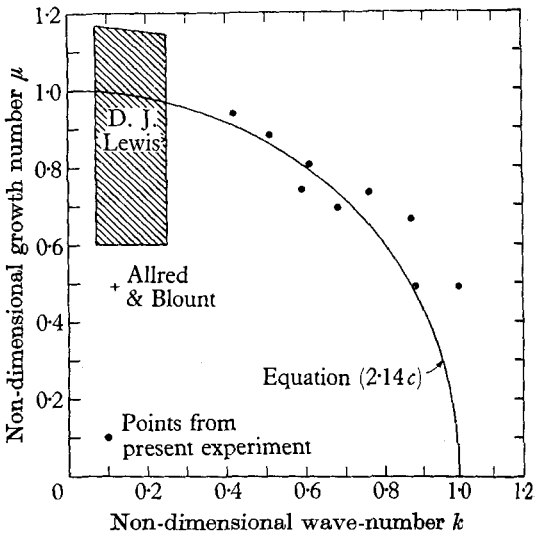

FIGURE 9. Initial growth rate.

C. *Experimental results on surface waves, small amplitudes*

The results of initial growth-rate experiments can best be discussed with the aid of figure 9 which is based on two non-dimensional numbers μ, a measure of the rate of wave-amplitude increase, as the ordinate and k, the ratio of wave-number to the cut-off wave-number, as abscissa.

For $k < 1$ the predominate growth rate is that predicted by the linear theory of Bellman & Pennington (1954) and given here by equations 2.14*b* and 2.14*c*. This linear theory prediction is represented by a solid line forming a quarter circle in the μ, k-plane of figure 9.

The value of μ from experimental results of wave growth in the $k < 1$ range is taken as the solution of the equation

$$\mu = \frac{1}{t_m} \cosh^{-1} \frac{\eta_m}{\eta_0}, \tag{2.21}$$

where η_m/η_0 is the ratio of the measured height to the initial wave height (for experimental convenience the double amplitude or crest-to-trough distance is used) and t_m is the non-dimensional time at which the wave reached the height η_m.

If the results of a large number of experiments performed by Lewis (1950) of a water-air interface are interpreted by the above method, then these results will fall in the shaded area of figure 9. As a result of the large accelerations and moderately long wavelengths used by Lewis the effects of surface tension would not be expected to be revealed.

The single point placed by the names, Allred & Blount, represent the results of an experiment reported by them in which they used n-heptane and air as the two fluids. Unfortunately, this is the only experiment of this type reported by them; their other experiments involved the interface between two fluids with densities close to each other in value and, therefore, cannot be represented entirely as functions of the two dimensionless numbers used in this figure.

Film	k' cm^{-1}	g'/g	k	$\eta_0 k_c$	μ
D-3	8·64	2·32	1·00	0·11	0·49
H-4	5·91	2·18	0·68	0·098	0·57
M-7	6·64	2·24	0·76	0·11	0·64
H-10	7·00	1·86	0·87	0·12	0·62
H-11	7·26	1·96	0·88	0·024	0·46
K-2	7·77	6·81	0·51	0·064	0·63
L-1	9·37	6·86	0·61	0·046	0·63
L-3	6·53	6·94	0·42	0·032	0·61
L-6	9·04	6·96	0·59	0·15	0·57

TABLE 2. Initial wave-growth data

The rest of the points in figure 9 are the results of the present work; the dimensional wave-numbers and accelerations of the experimental runs corresponding to the points in the μ, k-plane are given in table 2. Although there is a definite decrease in growth rate as the wave-number approaches cut-off, all the photographs of initially disturbed surfaces showed some evidence of wave growth. The experimental scatter is largely due to inaccuracies in the determination of the initial amplitudes.

Beyond the cut-off wave-number as shown in figure 10 (plate 3) there is an indication of a type of behaviour here called over-stability. The photographs taken of wave growth under these conditions indicate a standing oscillation of the waves with amplitude increasing in time. In figure 10 the points A, B and C designate the same position in the space of the frame, and it is seen that the waves have been caught in different positions of oscillation.

No more than a single oscillation has been observed; apparently after passing through one reversal of direction the wave grows to a large size and well-developed third-stage growth appears with the resulting competition between bubbles soon reducing the number of bubbles in a given space. There is some evidence that the larger the value of k for waves behaving in the over-stable manner, the higher the frequency at which the wave oscillates, as would be expected from equation (2.14c).

D. *Later stage wave-growth experiments*

The films which were analysed for third-stage growth showed considerable scatter of results even though a selective process was applied in the choice of which group of waves were to be studied; i.e. those waves were chosen which

appeared to be in a group of waves of a fairly uniform nature. The scatter was largely due to two things: the presence of odd modes of vibration imposed on the steady growth, and to small variations in initial conditions which become magnified at later times.

Except for the prediction of over-stability, the third-order theory does not check well with the experimental results. The theory predicts an ever-growing oscillation while the experiments never show more than one cycle of oscillation

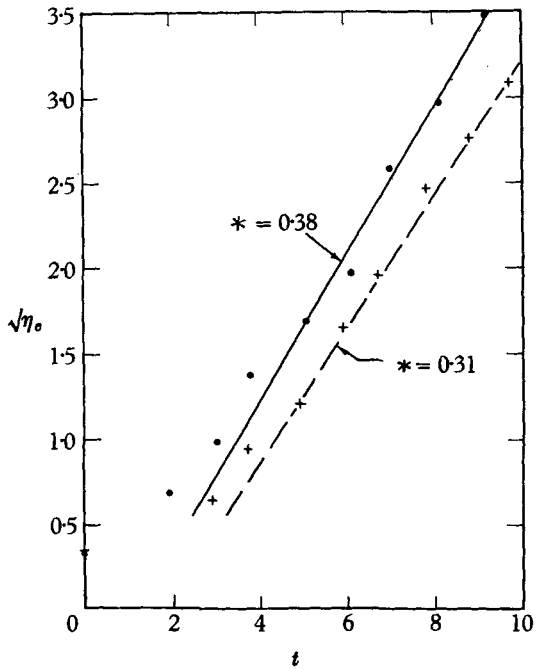

FIGURE 11. Spike acceleration. $* = \dfrac{\text{Spike acceleration}}{\text{Acceleration of free fall}}$

before monotonic growth occurs. It is not known at present whether the inadequacy is in the theoretical treatment or in the experimental boundary conditions.

Spike acceleration is illustrated by figure 11. Of the photographs measured for spike growth all indicated an acceleration of less than half the rate of free fall in the particular virtual gravity field applied. This may be compared with Carrier's (1953) work and the machine calculations of Pennington *et al.* (1953), which indicated a rate of acceleration equal to the free-fall rate. Since both of these theoretical predictions assume the surface tension to be zero, they would indicate a higher rate of growth because the surface tension forces act against the direction of acceleration of the spikes.

On the other hand, experimental results on bubble velocity resulted in good agreement with the theoretical predictions. The results, which are illustrated by two examples given in figure 12, in general give the conclusion that the value of c in the equation, $v = c\sqrt{g\lambda}$, lies between 0·2 and 0·3. This agrees with the theory

of Birkhoff (1954) and the work of Garabedian (1957), even though they did not consider surface tension effects in their analyses.

Examples of competition between bubbles are observed in every photograph taken of the wave disturbance type.

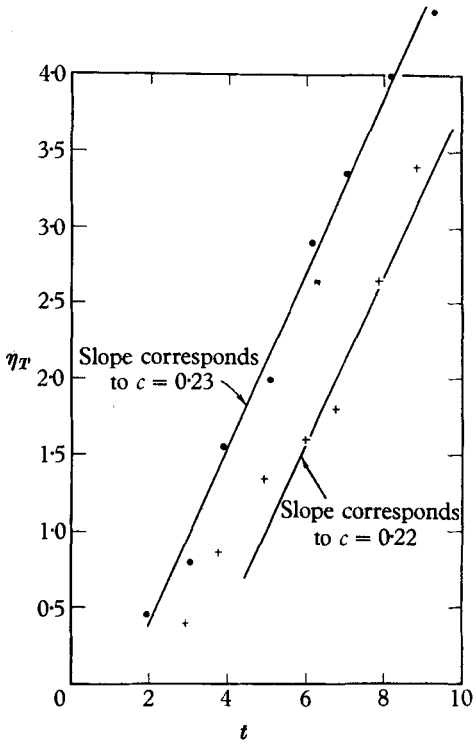

FIGURE 12. Bubble velocity.

3. Experiments involving a liquid sheet at the wall

If the surface is not disturbed by the vibrating paddle, a distortion of the surface still results from the liquid meniscus around the edge of the accelerated container as is illustrated by figure 13 (plate 4). Point A is the position reached by a very thin sheet of liquid next to the glass. Point B is the top of a thin wall of liquid that is in the exact centre between the glass walls. Points C and D are the tips of two two-dimensional bubbles which occupy the space between the sheets at the wall and the liquid wall in the centre. The more or less round bubbles of which there are four, one in each corner, are at the points E and F. The above is further illustrated by figure 14 (plate 5) in which an oblique view of the same type of phenomenon is offered.

Some study was made on the behaviour of the liquid sheet at the side wall. The results of this study are given in figure 15. Two liquids, methanol and carbon tetrachloride, were used in these experiments, and little difference was found between the two except that in the case of the carbon tetrachloride a second thickening of the sheet was seen to occur some distance back from the leading edge. This thickening was seen to catch up with the leading edge, after the leading-

edge acceleration began to slacken, and to provide fresh impetus allowing acceleration to continue at the original rate for a further distance. This point is illustrated by a comparison of figures 15 and 16. In figure 16 the line, labelled second wave line, represents the region where the thickening has caught up with the leading edge.

A graph, figure 17, of the ratio of the leading-edge acceleration to the applied gravity field versus the applied gravity field indicates that the leading edge

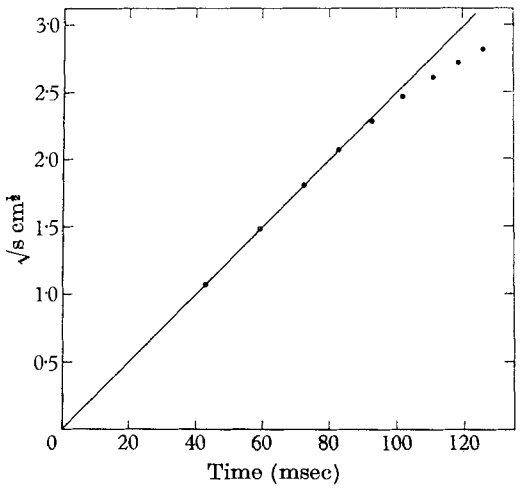

FIGURE 15. Square root of the relative displacement of the leading edge of the methanol sheet at the wall *vs* time.

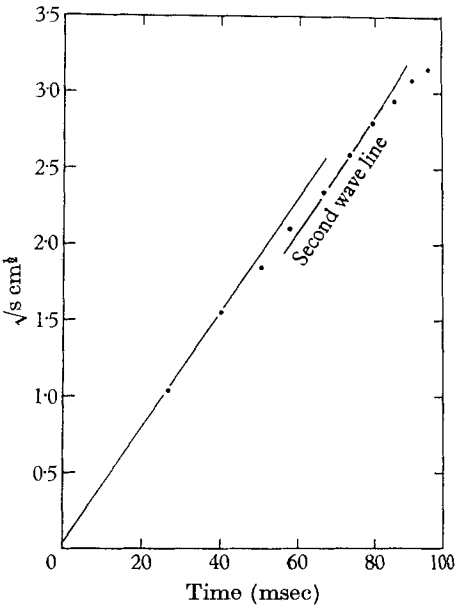

FIGURE 16. Square root of the relative displacement of the leading edge of the carbon tetrachloride sheet at the wall *vs* time.

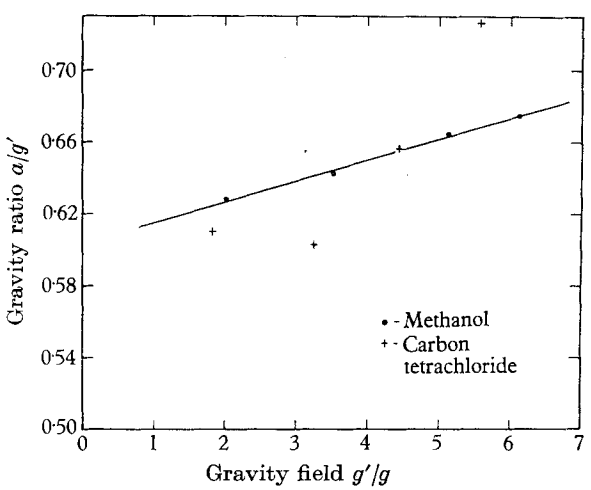

FIGURE 17. The ratio of the acceleration of the leading edge of the liquid sheet at the wall to the acceleration of free fall in the applied gravity field *vs* the applied gravity field.

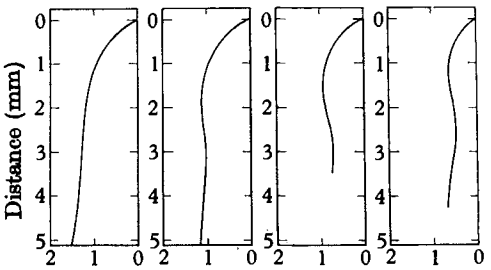

Time (msec)	43·7	60·0	72·8	83·3
Displacement (cm)	1·17	2·22	3·30	4·30

FIGURE 18*a*. Liquid sheet profiles at a low acceleration rate.

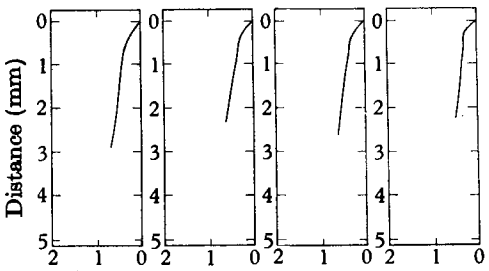

Time (msec)	38·2	46·5	53·9	59·8
Displacement (cm)	3·12	4·40	5·80	7·09

FIGURE 18*b*. Liquid sheet profiles at a high acceleration rate.

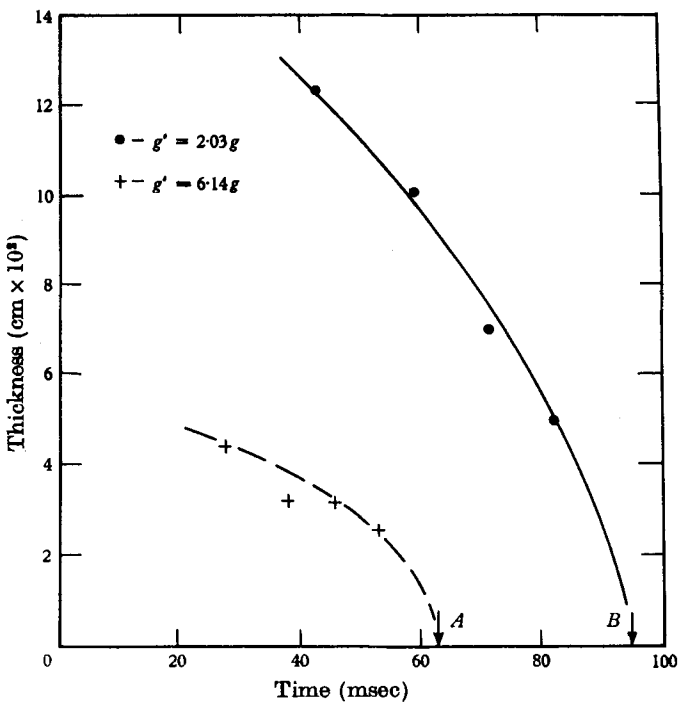

FIGURE 19. Profile thickness.

travels, in the ranges of applied gravities used here, at from 0·6 to 0·7 as fast as a free falling body. This is a higher acceleration than any observed in the case of wave spikes.

In order to get more information on the manner in which the accelerating sheet acts, the profiles of the sheet at the wall were determined at the highest and lowest rates at which the experiments with methanol were run. These results are given in figures 18*a* and 18*b*.

From the profile, a characteristic thickness can be measured and plotted versus time as in figure 19. The points marked A and B in this figure represent the time at which the displacement of the leading edge no longer maintained its constant acceleration. From this it can be deduced that at the time A for the experiment giving the profile shown in figure 18*a* and at the time B for the experiment giving the profile shown in figure 18*b* the liquid sheet ran out of fluid in the sense that the rate of supply from the main body of liquid was insufficient to allow things to continue as they had been.

The authors gratefully acknowledge the support of this work by the Office of Ordnance Research, U.S. Army, through Combustion Research Contract No. DA-19-920-ORD-1029.

Appendix I

Amplitudes of forcing functions of the third approximation, equation (2.14*h*, *i*)

$$P_{31}(t) = -\frac{\mu_1}{32}\left\{\frac{32(\mu_1/\mu_2)^4 - 8(\mu_1/\mu_2)^2 - 3}{4(\mu_1/\mu_2)^2 - 1}\right\}\sinh(\mu_1 t) + \frac{\mu_1}{32}\left\{\frac{3 - 8(\mu_1/\mu_2)^2}{4(\mu_1/\mu_2)^2 - 1}\right\}\sinh(3\mu_1 t)$$
$$+\frac{\mu_1-\mu_2}{2}\frac{(\mu_1/\mu_2)^4}{4(\mu_1/\mu_2)^2-1}\sinh(\mu_1+\mu_2)t + \frac{\mu_1+\mu_2}{2}\frac{(\mu_1/\mu_2)^4}{4(\mu_1/\mu_2)^2-1}\sinh(\mu_1-\mu_2)t,$$

$$P_{33}(t) = \frac{\mu_1}{32}\left\{\frac{96(\mu_1/\mu_2)^4 - 48(\mu_1/\mu_2)^2 + 9}{4(\mu_1/\mu_2)^2 - 1}\right\}\sinh(\mu_1 t) + \frac{9}{32}\frac{\mu_1}{4(\mu_1/\mu_2)^2-1}\sinh(3\mu_1 t)$$
$$-\tfrac{3}{2}(\mu_1+\mu_2)\frac{(\mu_1/\mu_2)^4}{4(\mu_1/\mu_2)^2-1}\sinh(\mu_1+\mu_2)t - \tfrac{3}{2}(\mu_1-\mu_2)\frac{(\mu_1/\mu_2)^4}{4(\mu_1/\mu_2)^2-1}\sinh(\mu_1-\mu_2)t.$$

$$Q_{31}(t) = -\left\{\frac{9}{33}\frac{1-\mu_1^2}{\mu_1^2} - \frac{\mu_1^2}{32}\left[\frac{32(\mu_1/\mu_2)^4 - 1}{4(\mu_1/\mu_2)^2 - 1}\right]\right\}\cosh(\mu_1 t)$$
$$-\left\{\frac{3}{32}\frac{1-\mu_1^2}{\mu_1^2} - \frac{\mu_1^2}{32}\left[\frac{16(\mu_1/\mu_2)^2 + 5}{4(\mu_1/\mu_2)^2 - 1}\right]\right\}\cosh(3\mu_1 t)$$
$$-\tfrac{1}{2}(\mu_1+\mu_2)^2\frac{(\mu_1/\mu_2)^4}{4(\mu_1/\mu_2)^2-1}\cosh(\mu_1+\mu_2)t - \tfrac{1}{2}(\mu_1-\mu_2)^2\frac{(\mu_1/\mu_2)^4}{4(\mu_1/\mu_2)^2-1}\cosh(\mu_1-\mu_2)t,$$

$$Q_{33}(t) = \left\{\frac{9}{32}\frac{1-\mu_1^2}{\mu_1^2} + \frac{\mu_1^2}{32}\left[\frac{32(\mu_1/\mu_2)^4 - 8(\mu_1/\mu_2)^2 + 5}{4(\mu_1/\mu_2)^2 - 1}\right]\right\}\cosh(\mu_1 t)$$
$$+\left\{\frac{3}{32}\frac{1-\mu_1^2}{\mu_1^2} - \frac{\mu_1^2}{32}\left[\frac{8(\mu_1/\mu_2)^2 - 7}{4(\mu_1/\mu_2)^2 - 1}\right]\right\}\cosh(3\mu_1 t)$$
$$-\tfrac{1}{2}(\mu_1^2+\mu_2^2)\frac{(\mu_1/\mu_2)^4}{4(\mu_1/\mu_2)^2-1}\{\cosh(\mu_1+\mu_2)t + \cosh(\mu_1-\mu_2)t\}.$$

FIGURE 1. A later stage of wave development.

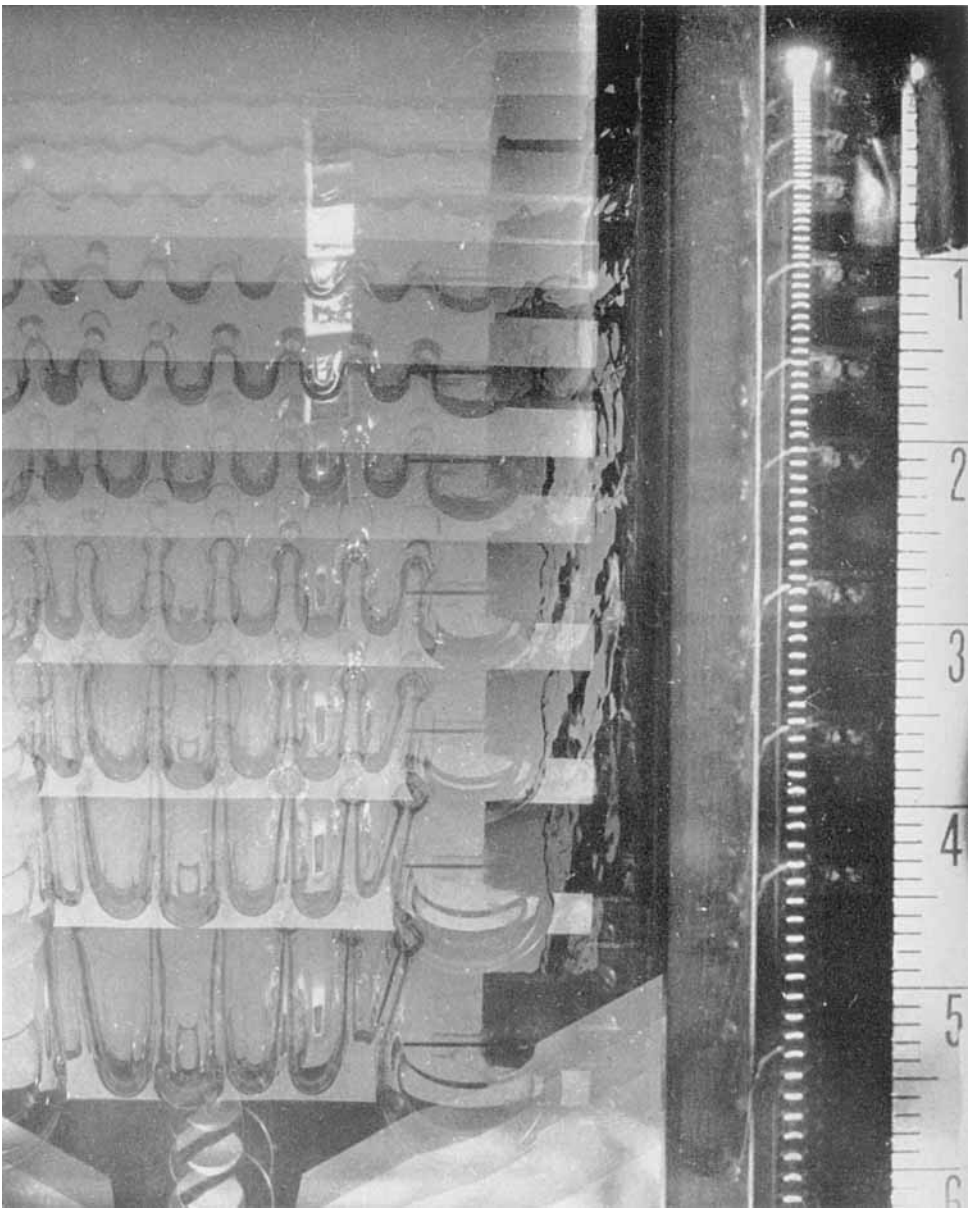

FIGURE 6. Typical photograph of position of interface at ten stages of growth.

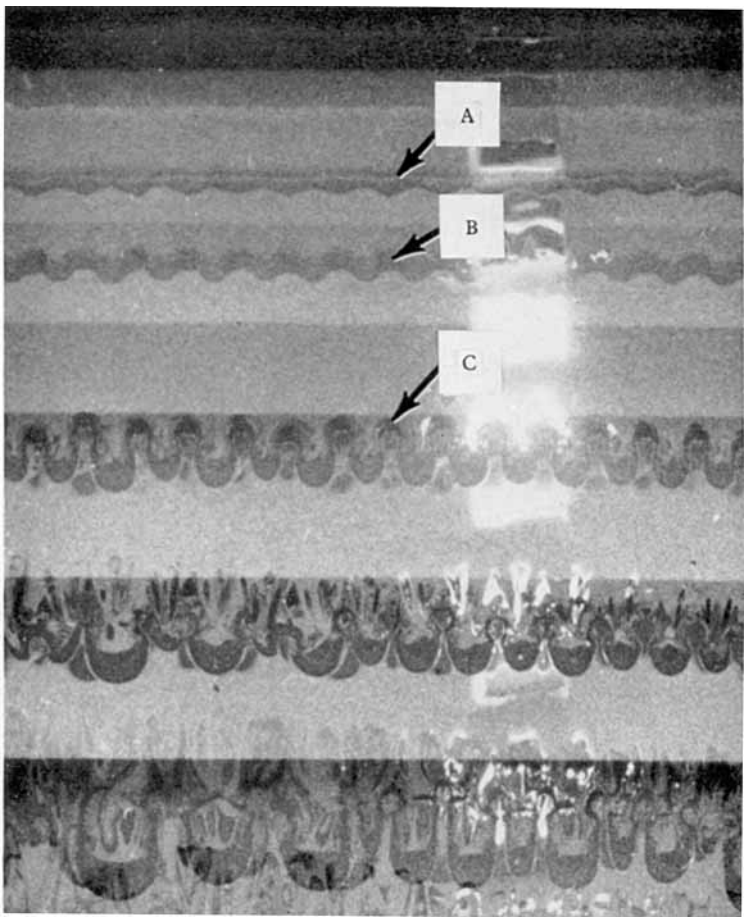

FIGURE 10. Example of over-stable growth.

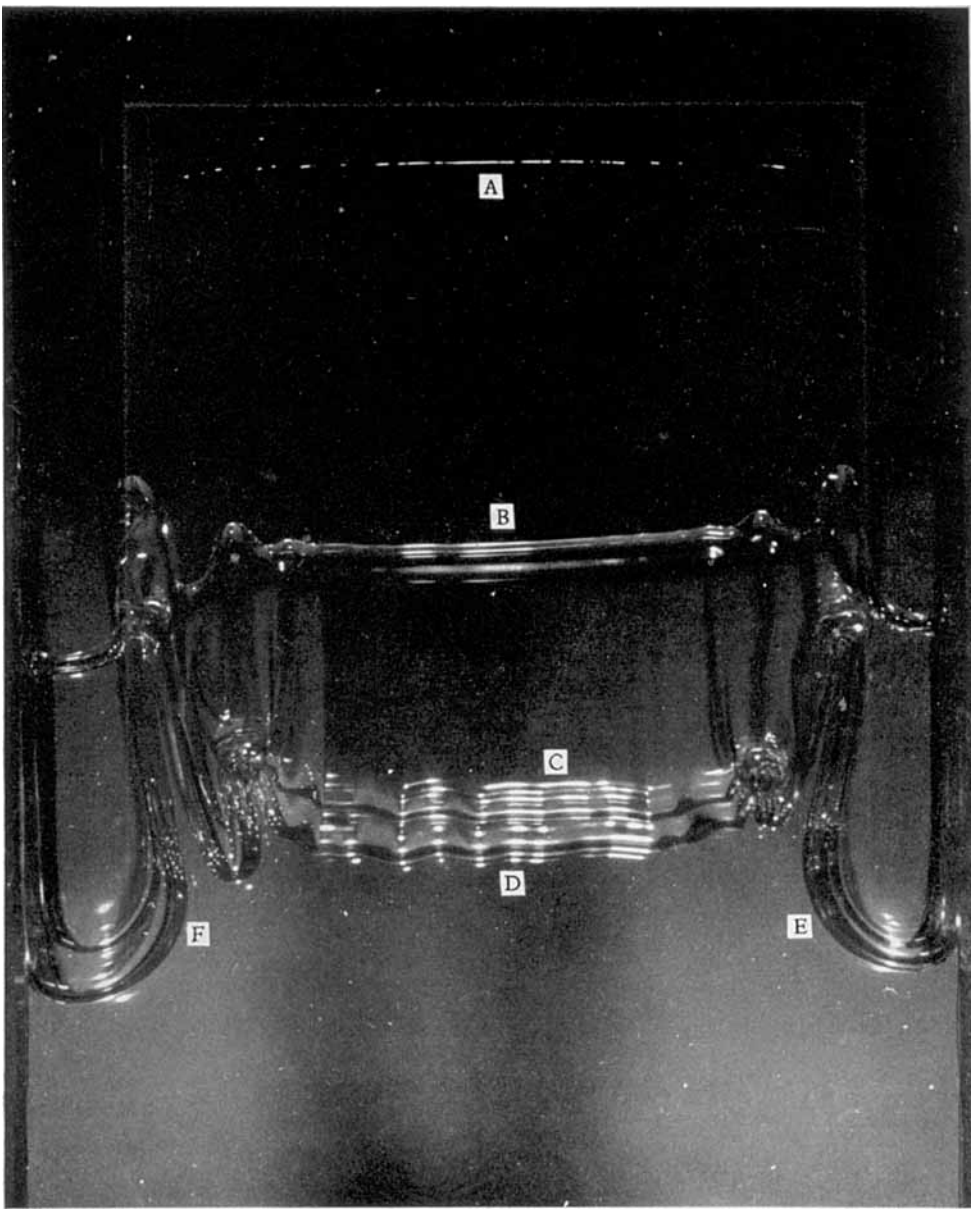

FIGURE 13. The growth of an initially undisturbed surface.

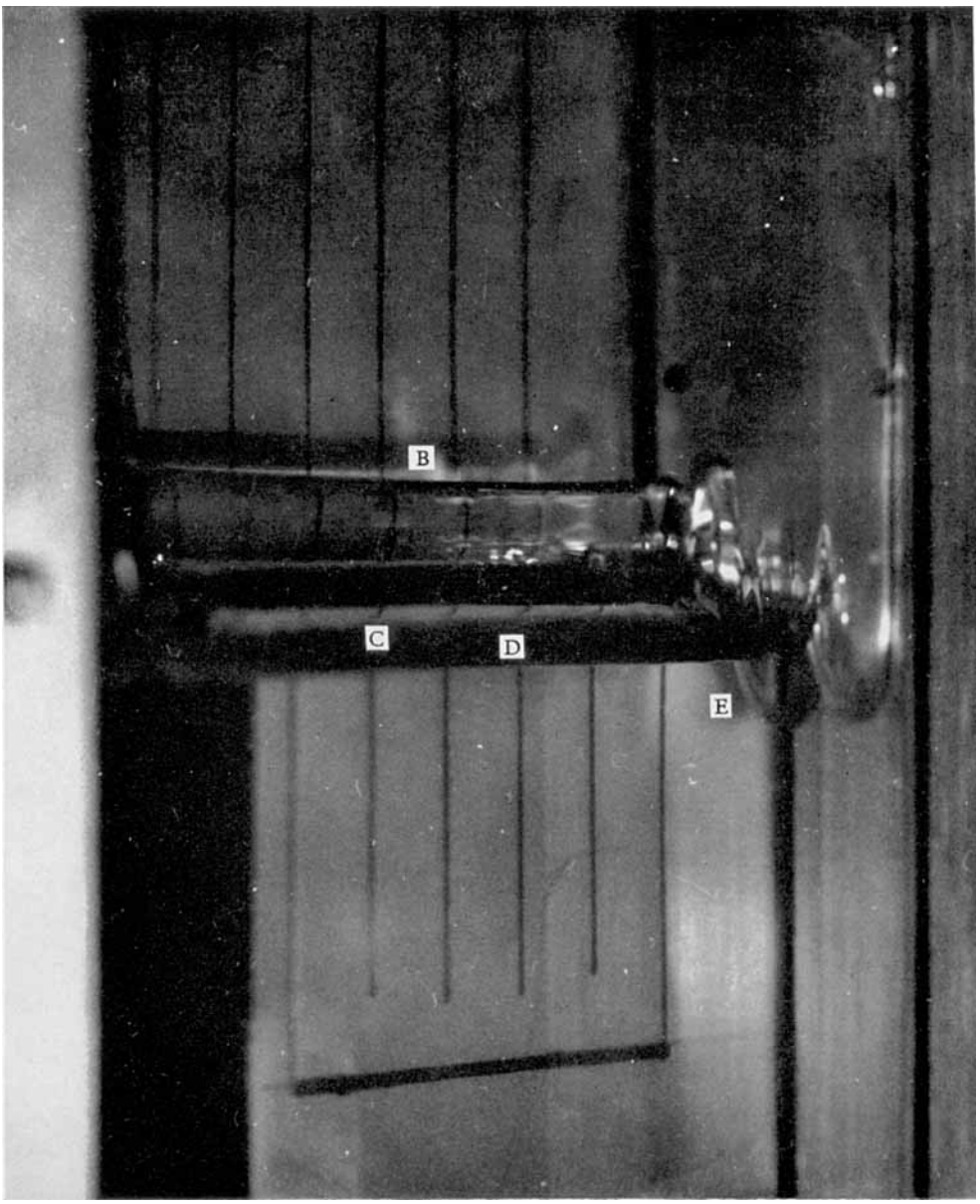

FIGURE 14. Oblique view of the growth of an initially undisturbed surface.

Appendix II

Amplitude functions of the third-stage approximation, equations (2.15) *and* (2.16)

$$C_{31}(t) = P_{31}(t) - B_{31}(t), \quad C_{33}(t) = P_{33}(t) - \tfrac{1}{3}B_{33}(t),$$

$$B_{31}(t) = a_{31}\cosh(\mu_1 t) + b_{31}\cosh(3\mu_1 t) + c_{31}\cosh(\mu_1 t)\cosh(\mu_2 t) + d_{31}\left(\frac{\mu_1}{\mu_2}\right)\sinh(\mu_1 t)\sinh(\mu_2 t) + e_{31}\mu_1 t\sinh(\mu_1 t),$$

$$B_{33}(t) = a_{33}\cosh(\mu_3 t) + b_{33}\cosh(3\mu_1 t) + c_{33}\cosh(\mu_1 t)\cosh(\mu_2 t) + d_{33}\left(\frac{\mu_1}{\mu_2}\right)\sinh(\mu_1 t)\sinh(\mu_2 t) + e_{33}\cosh(\mu_3 t),$$

where $P_{31}(t)$ and $P_{33}(t)$ are given in Appendix I, $\mu_r^2 = r(1-r^2k^2)$, and

$$a_{31} = -(b_{31}+c_{31}), \quad b_{31} = \frac{1}{8}\left\{\frac{3}{32}\frac{1-\mu_1^2}{\mu_1^2} - \frac{1}{4}\left[\frac{5(\mu_1/\mu_2)^2-1}{4(\mu_1/\mu_2)^2-1}\right]\right\},$$

$$c_{31} = 2\frac{(\mu_1/\mu_2)^6}{[4(\mu_1/\mu_2)^2-1]^2}, \quad d_{31} = 2\left(\frac{\mu_1}{\mu_2}\right)^4\frac{2(\mu_1/\mu_2)^2-1}{[4(\mu_1/\mu_2)^2-1]^2},$$

$$e_{31} = \frac{9}{64}\frac{1-\mu_1^2}{\mu_1^2} - \frac{1}{16}\left[\frac{16(\mu_1/\mu_2)^4 - 2(\mu_1/\mu_2)^2 - 1}{4(\mu_1/\mu_2)^2-1}\right],$$

$$a_{33} = -\frac{1}{1-(\mu_3/\mu_1)^2}\left\{\frac{27}{32}\frac{1-\mu_1^2}{\mu_1^2} + \frac{3}{16}\frac{4(\mu_1/\mu_2)^2+1}{4(\mu_1/\mu_2)^2-1}\right\},$$

$$b_{33} = -\frac{1}{9-(\mu_3/\mu_1)^2}\left\{\frac{9}{32}\frac{1-\mu_1^2}{\mu_1^2} - \frac{3}{16}\frac{4(\mu_1/\mu_2)^2+1}{4(\mu_1/\mu_2)^2-1}\right\},$$

$$c_{33} = 12\frac{(\mu_1/\mu_2)^2}{4(\mu_1/\mu_2)^2-1}\frac{1}{(\mu_3/\mu_1)^4 - 2[1+(\mu_2/\mu_1)^2](\mu_3/\mu_1)^2 + [1-(\mu_2/\mu_1)^2]^2},$$

$$d_{33} = -6\frac{(\mu_1/\mu_2)^2}{4(\mu_1/\mu_2)^2-1}\frac{1+(\mu_2/\mu_1)^2-(\mu_3/\mu_1)^2}{(\mu_3/\mu_1)^4 - 2[1+(\mu_2/\mu_1)^2](\mu_3/\mu_1)^2 + [1-(\mu_2/\mu_1)^2]^2}.$$

REFERENCES

ALLRED, J. & BLOUNT, G. 1953 Experimental studies of Taylor instability. *Report Los Alamos Scientific Laboratory of the University of California*, no. LA-1600.

BELLMAN, R. & PENNINGTON, R. H. 1954 Effects of surface tension and viscosity on Taylor instability. *Quart. J. Appl. Math.* **12**, 151.

BIRKHOFF, G. 1954 Taylor instability and laminar mixing. *Report Los Alamos Scientific Laboratory of the University of California*, no. LA-1862.

CARRIER, G. F. 1953 On Taylor instability with large motions. *Un-numbered report Los Alamos Scientific Laboratory of the University of California.*

DAVIES, R. M. & TAYLOR, G. I. 1950 The mechanics of large bubbles rising through extended liquids and through liquids in tubes. *Proc. Roy. Soc.* A, **200**, 375.

GARABEDIAN, P. R. 1957 On steady state bubbles generated by Taylor instability. *Applied Mathematics and Statistics Laboratory, Stanford University, Tech. Rep.* no. 59.

INGRAHAM, R. L. 1954 Taylor instability of the interface between superposed fluids. *Proc. Phys. Soc. Lond.* B, **67**, 748–52.

LEWIS, D. J. 1950 The instability of liquid surfaces when accelerated in a direction perpendicular to their planes. II. *Proc. Roy. Soc.* A, **202**, 81–96.

PENNINGTON, R. *et al.* 1953 Machine calculation of the growth of Taylor instability in an incompressible fluid. *Project Matterhorn Report*, no. PNJ-LA-11, p. 659.

TAYLOR, G. I. 1950 The instability of liquid surfaces when accelerated in a direction perpendicular to their planes. I. *Proc. Roy. Soc.* A, **201**, 192–6.